Impact of sodium excess on electrical conductivity of $Na_{3+x}Zr_2Si_2PO_{12+x/2}$ ceramics

Sahir Naqash[1-3*], Frank Tietz[1-3], E. Yazhenskikh[2,4], M. Müller[2,4], Olivier Guillon[1-3]

1. Forschungszentrum Jülich GmbH, Institute of Energy and Climate Research, Materials Synthesis and Processing (IEK-1), 52425 Jülich, Germany;
2. Jülich Aachen Research Alliance, JARA-Energy;
3. Helmholtz-Institute Münster, Forschungszentrum Jülich GmbH, 52425 Jülich, Germany
4. Forschungszentrum Jülich GmbH, Institute of Energy and Climate Research, Microstructure and Properties of Materials (IEK-2), 52425 Jülich, Germany;

Abstract

In order to industrialize NaSICON materials, modern fabrication techniques have to be used and one of those techniques for producing large-scale electrolyte sheets with 10-300 µm thickness is tape casting. Such technique however requires a sintering step at high temperatures for fabrication of ceramic components leading to sodium depletion due to evaporation. The sodium loss becomes more significant for large-area and thin components. In order to investigate and compensate the sodium loss, NaSICON compositions with a sodium excess were prepared, i.e. $Na_{3+x}Zr_2Si_2PO_{12}$ ($0 \leq x \leq 0.4$). The sodium loss can be reduced by applying a two-step sintering process (1250 °C for only 0.5 h and then at 1230 °C for 5 h). Several characterization techniques were used to analyze the resulting ceramics, the sodium depletion and its consequence on electrical conductivity. Chemical analyses indicated that all compositions were sodium deficient. Furthermore, the weight loss was investigated by thermogravimetric analysis confirming the reduction of weight loss by a factor 2 by applying a two-step sintering procedure with lower second sintering temperature. Initial thermodynamic calculations of the phase equilibria at high temperatures confirm the predominant evaporation of sodium. The highest electrical conductivity ($1.6 \cdot 10^{-3}$ S cm^{-1} at 25 °C) was measured for the composition showing the least sodium deficiency ($x = 0.2$). Furthermore, the activation energy of bulk and grain boundary conductivity decreased with increasing x in system.

1. Introduction

The sodium superionic-conducting ceramic (NaSICON) with composition $Na_3Zr_2Si_2PO_{12}$ [1, 2] has been investigated during recent decades due to the high ionic conductivity making the material a suitable option as a solid electrolyte in batteries or other electrochemical devices. A wide variation of substitutions were performed in this family of compositions and are reviewed in [3].

The structure of NaSICON consists of a three-dimensional framework of corner-sharing MO_6 octahedra and PO_4 tetrahedra. Contrary to the common opinion, not all NaSICON materials have the same crystal structure. Depending on their composition, sodium- or lithium-based NaSICON materials are most commonly either rhombohedral or monoclinic. Some triclinic NaSICON materials have also been reported as the low-temperature phase of $LiZr_2(PO_4)_3$ [4] or $LiSn_2(PO_4)_3$ [5]. The series $Na_{1+x}Zr_2Si_xP_{3-x}O_{12}$ ($0 \leq x \leq 3$) has a rhombohedral structure (space group $R\bar{3}c$) except when $1.8 \leq x \leq 2.2$. In this interval, the material undergoes a monoclinic distortion with space group ($C2/c$).

The conductivity of NaSICONs also varies with varying the crystal structure. The monoclinic distortion in $Na_3Zr_2Si_2PO_{12}$ leads to an increase in conductivity by two orders of magnitude [2]. However, crystal structure is not the only factor influencing the conductivity. Other factors such as charge carrier concentration (Na^+) and cation substitution of Zr^{4+} with transition metal ions also have a strong influence. As an example, partial substitution of Zr^{4+} with Sc^{3+} increases the conductivity as high as 4 mS cm^{-1} [6]. Charge carrier concentration directly influences the conductivity by simply enhancing the amount of mobile species in the system. Nevertheless, vacancies are also vital for the ionic transport in the lattice, therefore a balance between Na^+ and vacancies must be reached for maximum conductivity. The balance is reported to be at 3.4 moles of Na per formula unit for $Na_{3+x}Sc_xZr_{2-x}(SiO_4)_2(PO_4)$ [6], $Na_{3+x}Sc_2Si_xP_{3-x}O_{12}$ [7] and $Na_{1+x}Zr_2Si_xP_{3-x}O_{12}$ [8].

Since the NaSICON materials contain volatile elements, especially sodium and phosphorous, they are prone to weight loss at elevated temperatures. It has been reported that after sintering above 1200 °C, $Na_3Zr_2Si_2PO_{12}$ suffers from sodium oxide loss [9]. This sodium loss also reduces

the charge carrier concentration in the material and consequently decreases its ionic conductivity (σ_{ion}) [7, 10, 11]. This can be avoided by two potential strategies. The first rather complicated strategy is by modification of the experimental sintering setup and the second is by controlling the chemistry. In the case of sintering setup, the sample needs to be encapsulated in a closed system in order to minimize the sodium oxide loss. For practical reasons the experimental conditions are simplified and many ceramics are sintered in a powder bed to protect the green body with coverage of powder composed of the same composition and sacrificed after the heat treatment. The second strategy is to control the chemistry by synthesizing $Na_3Zr_2Si_2PO_{12}$ with an excess of the volatile element. The excess amount would compensate the loss during sintering process. However, the weight loss is strongly dependent on the sintering temperature, dwell time and partial pressure of Na_2O and P_2O_5, i.e. the evaporation rates of the single oxides.

In this work, the second approach of improving σ_{ion} was followed by investigating the impact of an excess of sodium oxide in the series series $Na_{3+x}Zr_2Si_2PO_{12+x/2}$. The x was chosen as 0, 0.05, 0.1, 0.2, 0.3 and 0.4. Results of this study will be useful for optimizing the sodium loss during the sintering of tape-cast sheets. Additionally, it will also help understanding the impact of excess charge carriers on the conduction properties of the material.

2. Experimental

Nominal $Na_3Zr_2Si_2PO_{12}$ was prepared by the solution-assisted solid state reaction (SA-SSR) [12], where stoichiometric amounts of $NaNO_3$ (99.5 %), $ZrO(NO_3)_2$ (99 %) and $Si(OC_2H_5)_4$ (99 %), supplied from VWR International, Belgium, were mixed and dissolved in a quartz glass container. After the nitrates were dissolved in the solution, a stoichiometric amount of tetraethyl orthosilicate, $Si(OC_2H_5)_4$ was added. When the $Si(OC_2H_5)_4$ was hydrolyzed, a corresponding amount of $NH_4H_2PO_4$ was added and stirred for 30 minutes to form a homogeneous precipitation. The mixture was stirred overnight with 300 rpm at 50 °C. The homogenized mixture was firstly heated from 50 up to 100 °C to slowly evaporate the water. Subsequently, the product was fired in a furnace at 600 °C for 5 h to form an amorphous raw powder. During this heat treatment, the inorganic polymer matrix was pyrolyzed and NO_x, CO_2, H_2O evolved as

gaseous products. Afterwards the raw powder was calcined at 800 °C for 12 h and balled-milled on a roller bench for 48 h using zirconia balls. The milled powder was pressed into pellets (diameter =13 mm, thickness = 1.1-1.2 mm) with a pressure of ~150 MPa. After pressing, all samples showed similar green densities, i.e. 59 – 61 % of theoretical density. The pellets were sintered at different conditions including a two-step sintering (1250 °C for 0.5 h followed by 1230 °C for 5 h) with a heating and cooling rate of 5 K min^{-1}. These temperatures were chosen because sintering at higher temperature results in sample deformation due to partial melting.

After sintering the pellets were sputtered with gold as blocking electrodes. The electrical conductivity was measured by an impedance spectroscopy system (Biologic, VMP-300) from -30 °C to 100 °C.

The phase purity of the sintered specimens was measured by X-ray diffraction (XRD, Bruker D4 ENDEAVOR diffractometer with Cu K_α radiation), and the microstructure of the powder and pellet cross-sections was examined by scanning electron microscopy (SEM, Ultra55, Zeiss). Microstructural details like grain size distribution or fraction of porosity was determined using an image analysis software (analySIS pro, Olympus Soft Imaging Solutions GmbH, Version 5.0) The density of the samples was measured using an Ultrapycometer 1000, version 2.4 (Quantachrome Corporation), which uses gas displacement and the volume-pressure relationship (Boyle's law) to measure the density of the specimens. The particle size distribution was obtained using Horiba LA-950V2 laser diffraction particle size distribution analyzer with ethanol as dispersing medium.

The stoichiometry of the materials was controlled by inductively coupled plasma optical emission spectroscopy (ICP-OES) using the Thermo Scientific iCAP7600 spectrometer with optical scale and CID semi-conductor detector, axial und radial reflection, and wavelengths between 166 nm and 847 nm. 20 mg of powder were mixed to 0.25 g lithium borate in a platinum crucible and heated for 0.5 h at 1000 °C. The liquefied material was dissolved in 30 mL HCl (5 %). After dissolution, the sample solutions were transferred to sample vials containing 0.5 mL of HF and filled to 50 mL volume. Each test sample was diluted and measured twice.

Thermodynamic properties like vapor pressures of volatile species can be estimated with the help of thermodynamic calculations using appropriate software and thermodynamic databases. In the present work thermodynamic calculations were performed using the computational software package FactSage [13] with an in-house developed oxide database [14] combined with the

commercial database for pure gaseous substances (SGPS). The partial pressure of the main species is calculated under equilibrium conditions at 1250 °C. Since the ZrO_2-containing species are still not included into the database used, the data from the commercial database SGPS were implemented for condensed and gaseous phases. In this case the equilibrium calculations with ZrO_2 should be considered as preliminary values, because the formation and reactions with zirconia-containing phases are not taken into account in the database yet. The thermodynamic functions on the corresponding compounds are required in order to estimate the partial pressure over NaSICON. Since no thermodynamic data exist, the Gibbs energy functions have been generated based on the experimental data of Maier et al. [15]. The standard formation enthalpy and entropy as well as the temperature dependence of heat capacity were used.

3. Results and Discussion

3.1. Synthesis and Characterization

3.1.1. X-ray diffraction

The XRD patterns of the sintered samples of $Na_{3+x}Zr_2Si_2PO_{12+x/2}$ are shown in Fig. 1 between 2θ = 10° and 40°. All the compositions crystallized in the desired monoclinic C2/c NASICON structure. They all contained varying amounts of ZrO_2 as secondary phase, as depicted by blue vertical lines.

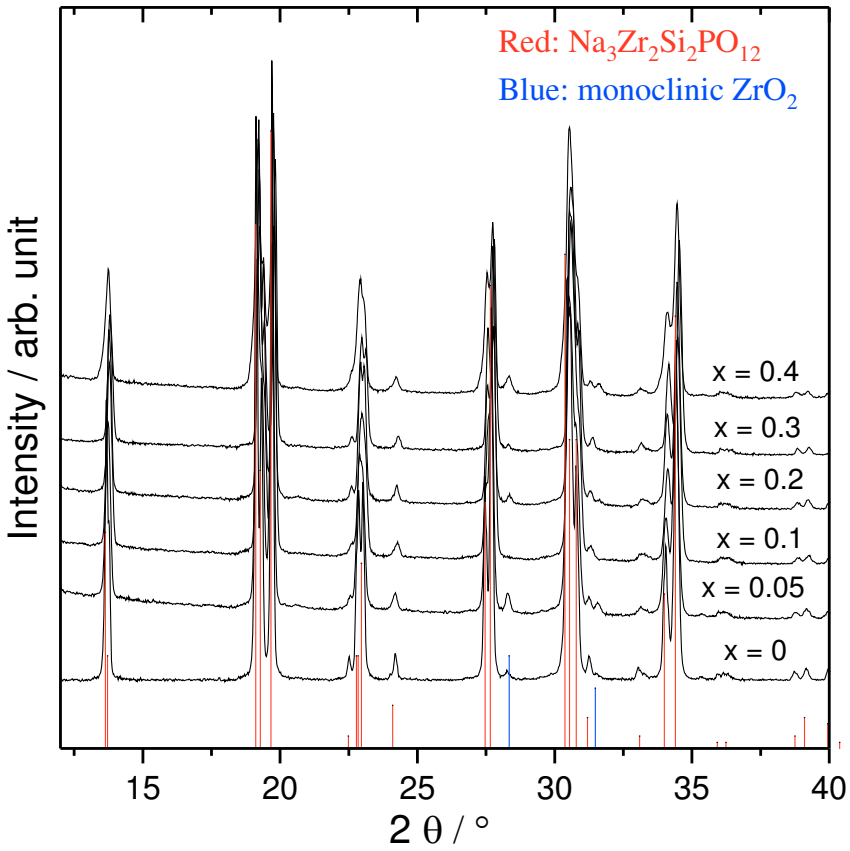

Fig. 1: The XRD patterns for the $Na_{3+x}Zr_2Si_2PO_{12+x/2}$ system at room temperature. The reference reflections of monoclinic ZrO_2 and $Na_3Zr_2Si_2PO_{12}$ were taken from [16] and [1], respectively.

The unit cell parameters of all compositions obtained by Rietveld refinement are given in Table 1. The results obtained in this study are comparable to reported values, e.g. for x = 0: a=15.586(9) Å, b=9.029(4) Å, c=9.205(5) Å, β=123.70(5)° and cell volume 1077.71(12) Å^3 [1, 17].

Table 1: The unit cell parameters of $Na_{3+x}Zr_2Si_2PO_{12+x/2}$.

NZSP$_x$	**a / Å**	**b / Å**	**c / Å**	**β / °**	**Volume / Å^3**
0	15.633(2)	9.011(1)	9.214(1)	123.70(6)	1079.05(6)
0.05	15.638(2)	9.049(1)	9.216(1)	123.76(1)	1084.26(8)
0.1	15.626(2)	9.043(1)	9.213(1)	123.72(1)	1082.82(8)
0.2	15.640(2)	9.050(1)	9.218(1)	123.76(1)	1084.69(6)

0.3	15.613(1)	9.034(1)	9.216(1)	123.62(1)	1082.52(6)
0.4	15.615(2)	9.035(1)	9.208(1)	123.69(1)	1080.96(8)

3.1.2. Powder characterization

After calcination, the powders were milled and the particle size distribution of milled powders is shown in Fig. 2. The particles sizes are classified in terms of d_{10}, d_{50} and d_{90} values, i.e. the diameter of particles obtained for 10, 50 and 90 % of all articles in a cumulative representation. All the powders have a similar d_{10} and d_{50} whereas the d_{90} has a relatively wider scatter. Furthermore, the PSD of the powders is similar and therefore any differences in the sintering process would not be due to the different sizes of initially pressed powders.

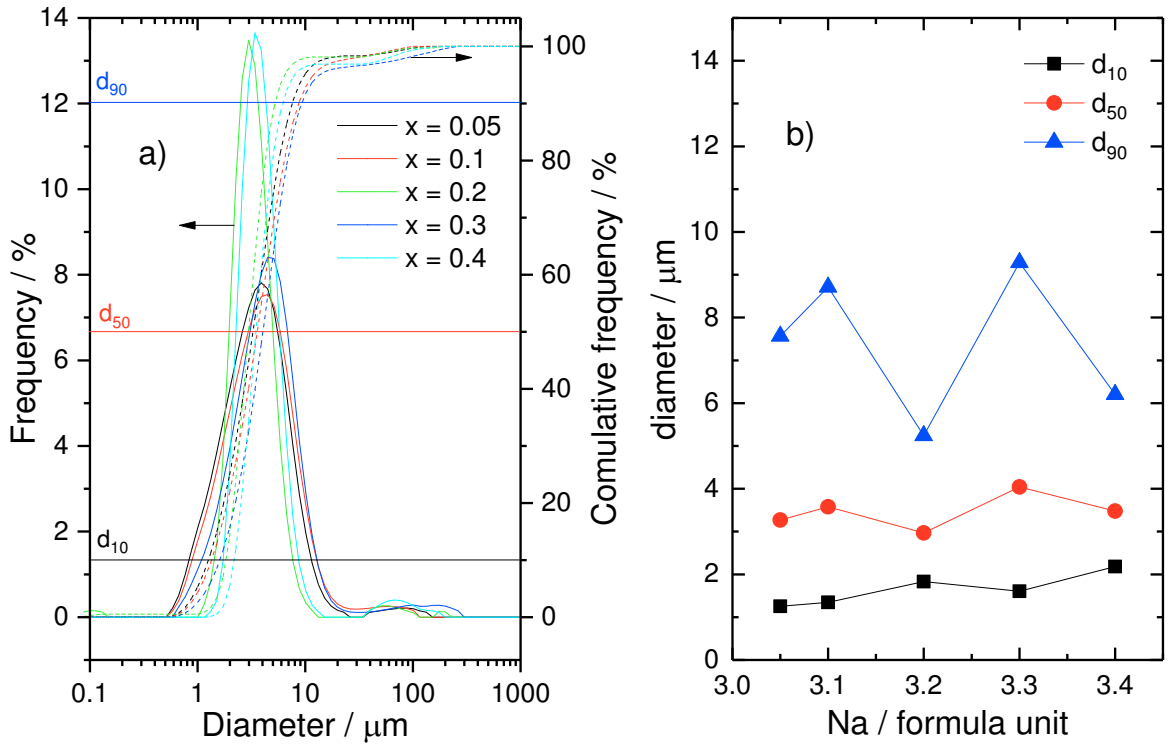

Fig. 2 a) The PSD of milled $Na_{3+x}Zr_2Si_2PO_{12+x/2}$ powders. b) Characteristic particles size diameters d_{10}, d_{50} and d_{90}.

3.1.3. Elemental Analysis (Stoichiometry)

The compositions in the series $Na_{3+x}Zr_2Si_2PO_{12+x/2}$ were chemically analyzed to control their accurate stoichiometry. Sodium content was found to be lower than anticipated, which is due to the hygroscopic nature of sodium starting material and sodium loss during sintering. The results are shown in Table 2 and Fig. 3a. The Zr content lies within the error limits of the measurement, whereas a systematic Si deficiency is arising from the starting material (TEOS).

Table 2: Nominal and analytical stoichiometry of sintered and crushed $Na_{3+x}Zr_2Si_2PO_{12+x/2}$.

Nominal	**Analytical (ICP-OES)**
$Na_{3.00}Zr_2Si_2PO_{12}$	$Na_{2.72}Zr_{2.06}Si_{1.97}PO_{11.92}$
$Na_{3.05}Zr_2Si_2PO_{12.025}$	$Na_{2.90}Zr_{2.00}Si_{1.83}PO_{11.61}$
$Na_{3.1}Zr_2Si_2PO_{12.05}$	$Na_{2.93}Zr_{1.99}Si_{1.81}PO_{11.57}$
$Na_{3.2}Zr_2Si_2PO_{12.1}$	$Na_{3.11}Zr_{2.01}Si_{1.84}PO_{11.76}$
$Na_{3.3}Zr_2Si_2PO_{12.15}$	$Na_{3.12}Zr_{2.00}Si_{1.84}PO_{11.74}$
$Na_{3.4}Zr_2Si_2PO_{12.2}$	$Na_{3.22}Zr_{1.94}Si_{1.68}PO_{11.35}$

The sodium content was further studied before milling and after sintering. Fig. 3b reveals that the Na content is lower than the anticipated nominal values in all cases. This systematic Na deficit is clearly because of the inaccurate starting calculation of sodium source ($NaNO_3$) and variation arise due to the hygroscopic nature of $NaNO_3$ [18]. In addition, a sodium loss during sintering process can also be seen. The sodium loss was negligible in the case of $Na_{3.2}Zr_2Si_2PO_{12.1.}$

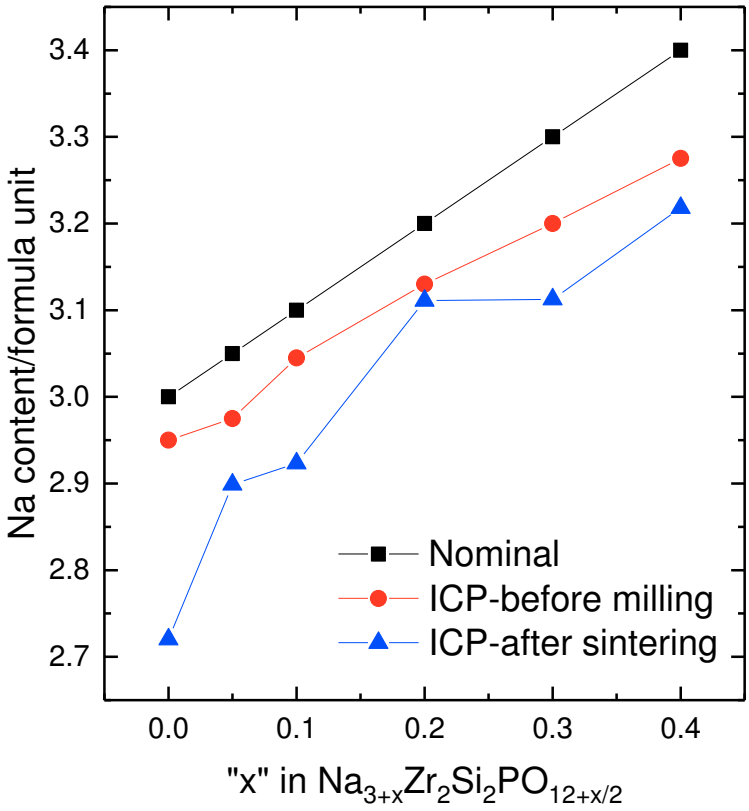

Fig. 3: The deviation of Na content before milling and after sintering. For better comparison, the results before milling and after sintering were normalized to the nominal phosphorous content. The sintering conditions were 1250 °C for 0.5 h, then 1230 °C for 5 h.

3.2. Sintering and Microstructure

3.2.1. Two-step Sintering

In a typical dilatometry curve, densification is rather a rapid phenomenon and occurs promptly before grain growth starts. To utilize this phenomenon, samples were first exposed to a high temperature for a short time (where densification occurs), which is followed by an elongated dwell time at reduced-temperature (where grain growth occurs). By using this sintering procedure the sodium loss is reduced because the sample remains at high temperature for only short time. This sintering route has already been used for other materials [19-21].

$Na_{3+x}Zr_2Si_2PO_{12+x/2}$ pellets were sintered by various sintering procedures and their resulting densities of the different attempts are shown in Fig. 4. Among which, the two-step sintering method (1250 °C for 0.5 h followed by 1230 °C for 5 h) resulted in reproducible relative densities of ≥ 90 % for all compositions. Therefore, this heat treatment sequence was applied to sinter all samples for further investigations.

A similar two-step sintering condition where samples were exposed to 1260 °C for 0.25 h followed by 1230 °C for 5 h produced high densities only when $x > 0.1$. The reason might be a synergic effect of i) very short exposure time at high temperature (1260 °C for 0.25 h) and ii) reduced sinterability of the ceramic due to less sodium content.

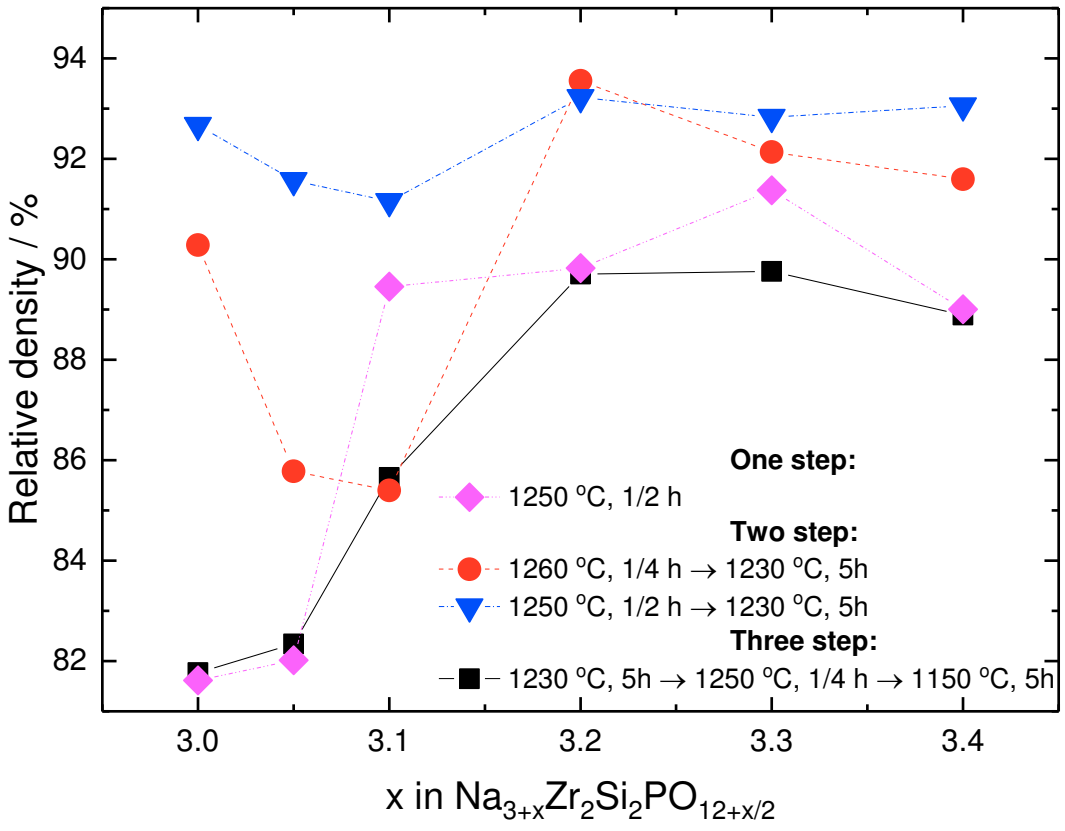

Fig. 4: Relative densities obtained after sintering applying different sintering conditions.

One-step and three-step sintering clearly fail to produce high densities particularly for $x = 0$ and $x = 0.05$. On the one hand the one-step sintering this is due to a too short exposure time at high temperature for the one step sintering that does not allow crystal growth process to take place. On the other hand the three step sintering process failed because the heating sequence is opposite to a typical sintering curve as described earlier in this section.

3.2.2. Microstructure

The microstructures of $Na_{3+x}Zr_2Si_2PO_{12+x/2}$ ceramics show that all compositions have similar grain sizes (Fig. 5). The secondary phase (ZrO_2) can also be seen as white particles, particularly in $Na_{3.05}Zr_2Si_2PO_{12.025}$ it exists in different morphologies such as cubic and monoclinic. The secondary phase is formed at inter-granular regions and seems to be embedded in an amorphous phase. The EDX analyses (not shown here) of this amorphous phase, which can be regarded as enlarged grain boundaries, confirmed that these regions are Zr deficient and Si rich. This is an evidence of the formation of a glassy phase as already discussed in a previous work [22] and reported by others [23-25]. This glassy phase is present only at the grain boundaries where it promotes the sinterability of NaSICON. Nonetheless it has a larger resistance than NaSICON and acts as an electrical barrier towards Na^+ conduction [26, 27].

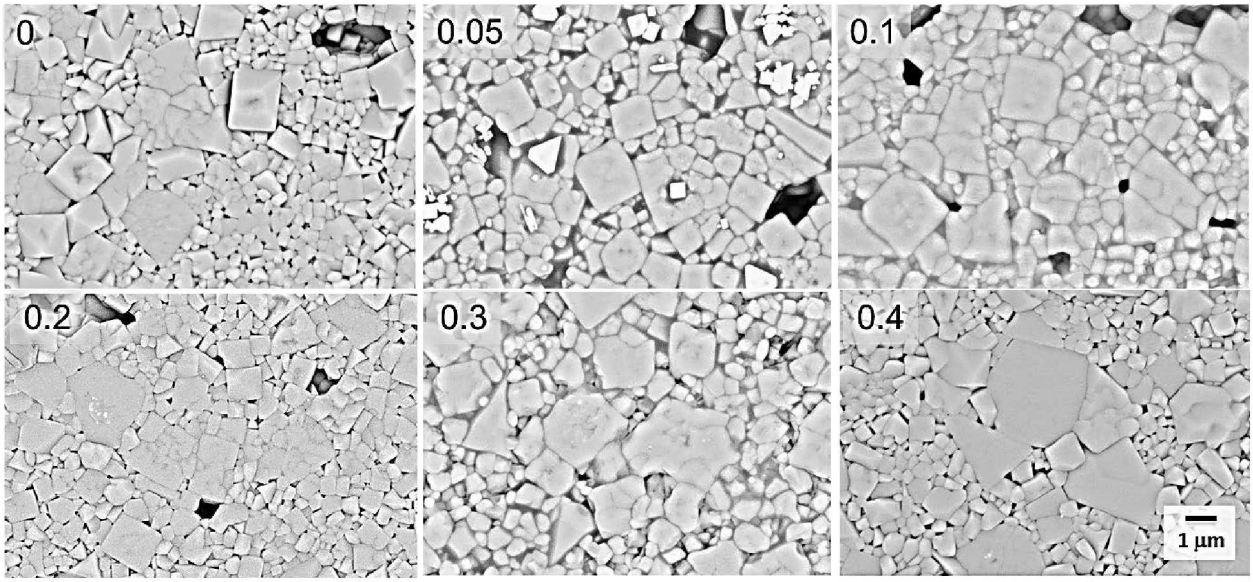

Fig. 5: Microstructure of $Na_{3+x}Zr_2Si_2PO_{12+x/2}$ ceramics obtained after two-step sintering and thermal etching at 1150 °C for 0.25 h.

3.3. Thermal investigation

DTA/TG measurements were performed and different sintering schedules were adopted and compared. The most important thermogravimetric observation was the weight loss during the holding time. This weight loss was more pronounced in case of a single hold at 1250 °C, here for 10 h, as compared to two dwell times at 1250 and 1230 °C as in the case of the two-step sintering Table 3). Not only the evaporation rates at both temperatures but also for the different compositions show that there is a significant variation in weight loss even if a very similar system is investigated. It is interesting to note that the largest weight loss was consistently measured for the $Na_{3.05}Zr_2Si_2PO_{12.025}$ sample, which also showed the highest amount of ZrO_2 in the microstructure. Whereas the evaporation rate of all other samples was nearly constant at 1250 °C, the values for the evaporation rates significantly increased for x = 0.3 and 0.4 at 1230 °C resulting in nearly the same rate as at 1250 °C. In these two cases the increase of the sodium concentration obviously has a stronger impact on the evaporation rates, whereas for 0 < x 0.2 the

evaporation rate is reduced by a factor of 2 to 3 when the sintering temperature is decreased by 20 °C.

Hence, the general assumption that a certain percentage in excess of the volatile element can compensate the losses during sintering is therefore in most applied cases not matching the real loss, either leading to a deficiency of the considered element or to a remaining excess in the specimens which may accumulate at the grain boundaries.

Table 3: Weight loss (in %) and evaporation rate (%/h) at 1250 and 1230°C.

x	$\Delta m_{1250°C,\ 10\ h}$	$\Delta m_{1250°C} / \Delta t$	$\Delta m_{1250\ °C,\ 0.5\ h \rightarrow 1230\ °C,\ 5\ h}$	$\Delta m_{1230°C} / \Delta t$
0	0.74	0.074	0.17	0.031
0.05	1.48	0.148	0.40	0.069
0.1	0.67	0.067	0.10	0.027
0.2	0.73	0.073	0.07	0.019
0.3	0.60	0.06	0.25	0.057
0.4	0.64	0.064	0.31	0.068

For better understanding of the different evaporation rates and weight losses of the specimens, initial thermodynamic calculations were carried out to determine the solid/gas equilibria and the vapor pressure of the volatile elements molecules in the system Na_2O-ZrO_2-SiO_2-P_2O_5. The main gaseous species over the pure oxides and mixture of them are given in Table 4. The volatility of Na_2O and P_2O_5 is noticeable, while silica and zirconia are characterized by high stability of the condensed phase. In the binary systems Na_2O-SiO_2 and Na_2O-P_2O_5, which have been thermodynamically assessed and the corresponding data have been included into the database used, all possible reactions between liquid, solid and gas phases are taken into account by the calculations. The partial pressure over the selected composition in the system Na_2O-P_2O_5 corresponds to that over Na_3PO_4 and not over the single initial oxides and is therefore significantly lower. In case of Na_2O:SiO_2=3:4 the equilibrium pressure is obtained over the liquid phase, which was calculated to be stable at 1250 °C. The partial pressure of Na is again lower than that over the pure oxide but higher than that over the phosphate. In case of the

composition in the ternary system Na_2O-P_2O_5-SiO_2, which is completely assessed, the partial pressure of Na is about to orders of magnitude higher than that of PO_2. The systems containing zirconia can be calculated only approximately; since the database for these systems is not complete, the properties of possible compounds and liquid phases are not taken into account. As a consequence, the vapor pressure of Na, O_2 and ZrO_2 is similar with that estimated over the pure oxides, phosphate or silicate melts. Similar limitations concern the calculation of equilibria between NaSICON compounds and gas phase, because the melting reaction or possible solid-solid transformations are not included in the preliminary dataset. Therefore, the predicted activity shows relatively high stability of these compounds accompanied by a low partial pressure of the main gaseous species.

Table 4: Partial pressures for gases in equilibrium with different solids or melts at 1250 °C

Equilibrium with single oxides	**Partial pressure (bar) of most volatile molecule or atom of each element**				
Na_2O (g)	Na $10^{-2.1}$	O_2 $10^{-2.7}$	-	-	-
SiO_2 (s)	-	O_2 $10^{-9.68}$	SiO $10^{-9.3}$	-	-
P_2O_5 (g)	-	O_2 $10^{-3.3}$	-	P_4O_{10} $10^{-0.0016}$	-
ZrO_2 (s)	-	O $10^{-15.8}$	-	-	ZrO $10^{-15.8}$
Equilibrium in binary system					
Na_2O – P_2O_5 (3:1)	Na $10^{-5.95}$	O_2 $10^{-6.42}$	-	PO_2 $10^{-6.44}$	-
Na_2O – SiO_2 (3:4)	Na $10^{-4.72}$	O_2 $10^{-5.32}$	SiO_2 $10^{-11.96}$	-	-
Na_2O – ZrO_2 (3:4) *	Na $10^{-2.1}$	O_2 $10^{-2.65}$	-	-	ZrO_2 $10^{-16.39}$
Equilibrium in ternary system					
Na_2O – P_2O_5 – SiO_2 (3:1:4)	Na $10^{-5.91}$	O_2 $10^{-6.5}$	SiO_2 $10^{-10.87}$	PO_2 $10^{-7.68}$	-
Na_2O – P_2O_5 – ZrO_2 (3:1:4)	Na $10^{-5.95}$	O_2 $10^{-6.42}$	-	PO_2 $10^{-6.44}$	ZrO_2 $10^{-16.39}$
Na_2O – ZrO_2 – SiO_2 (3:4:4)	Na $10^{-4.72}$	O_2 $10^{-5.32}$	SiO_2 $10^{-11.96}$	-	ZrO_2 $10^{-16.36}$
Equilibrium with individual compositions					
$NaZr_2P_3O_{12}$	Na	O_2	-	PO_2	ZrO_2 $10^{-8.11}$

$Na_{1+x}Zr_2Si_xP_{3-x}O_{12}$, x=0	$10^{-8.41}$	$10^{-8.33}$		$10^{-8.02}$	
$Na_3Zr_2Si_2PO_{12}$	Na	O_2	SiO	PO_2	ZrO_2
$Na_{1+x}Zr_2Si_xP_{3-x}O_{12}$, x=2	$10^{-8.77}$	$10^{-8.96}$	$10^{-8.97}$	$10^{-9.4}$	$10^{-8.94}$
$Na_4Zr_2Si_3O_{12}$	Na	O_2	SiO	-	ZrO_2
$Na_{1+x}Zr_2Si_xP_{3-x}O_{12}$, x=3	$10^{-8.93}$	$10^{-9.19}$	$10^{-9.08}$		$10^{-9.22}$

*: preliminary results, see experimental section

3.4. Electrical Conductivity

In the impedance diagrams of $Na_{3+x}Zr_2Si_2PO_{12+x/2}$ with $0 \leq x \leq 0.4$ only one semicircle can be measured at 25 °C which is not starting from zero-resistance (Fig. 6). This indicates that both bulk and grain boundaries contribute to the total resistance. The figure also indicates that the conductivity of the material is substantially influenced by the different sodium contents and $Na_{3.2}Zr_2Si_2PO_{12.1}$ has the highest bulk and total conductivity. This composition also contains minimum glass phase as observed from the microstructure.

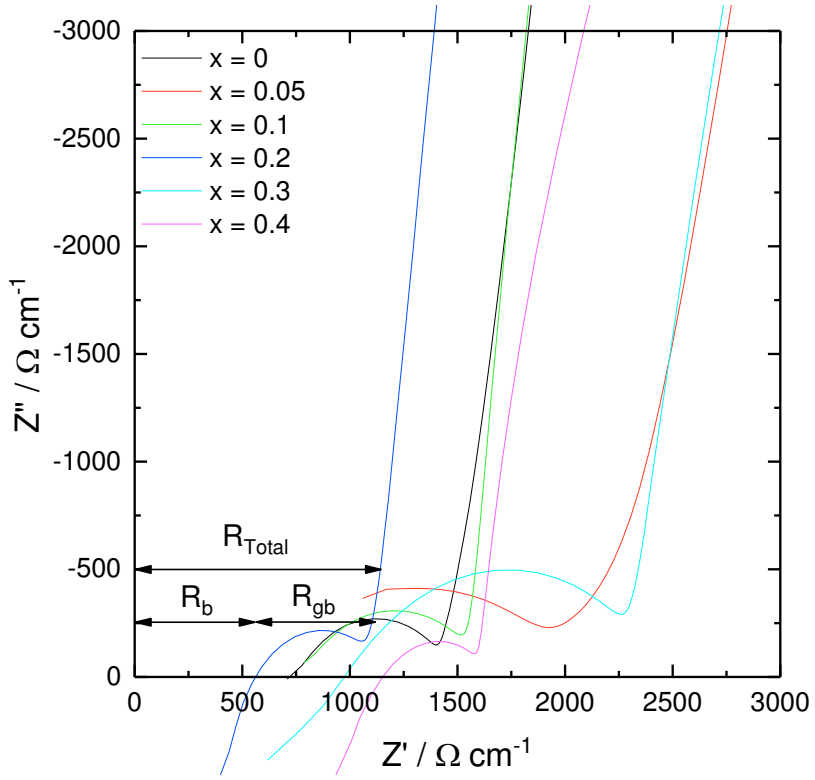

Fig. 6: Impedance spectra obtained at 25 °C for $Na_{3+x}Zr_2Si_2PO_{12+x/2}$ sintered at 1250 °C, 0.5 h and then 1230 °C for 5 h.

The Arrhenius plot of σ_{total} in the temperature range -30 – 100 °C is shown in Fig. 7 along with the activation energies (E_a). The different slopes in Fig. 7a indicate the different E_a values. The conductivity is highest for $Na_{3.2}Zr_2Si_2PO_{12.1}$ in the whole temperature range.

The E_a, when plotted against the Na content, shows a clear decreasing trend with an exception of $Na_3Zr_2Si_2PO_{12}$. Nevertheless, the whole range of activation energies of $Na_{3+x}Zr_2Si_2PO_{12+x/2}$ coincides with the reported range of E_a for various NaSICON materials [28, 29].

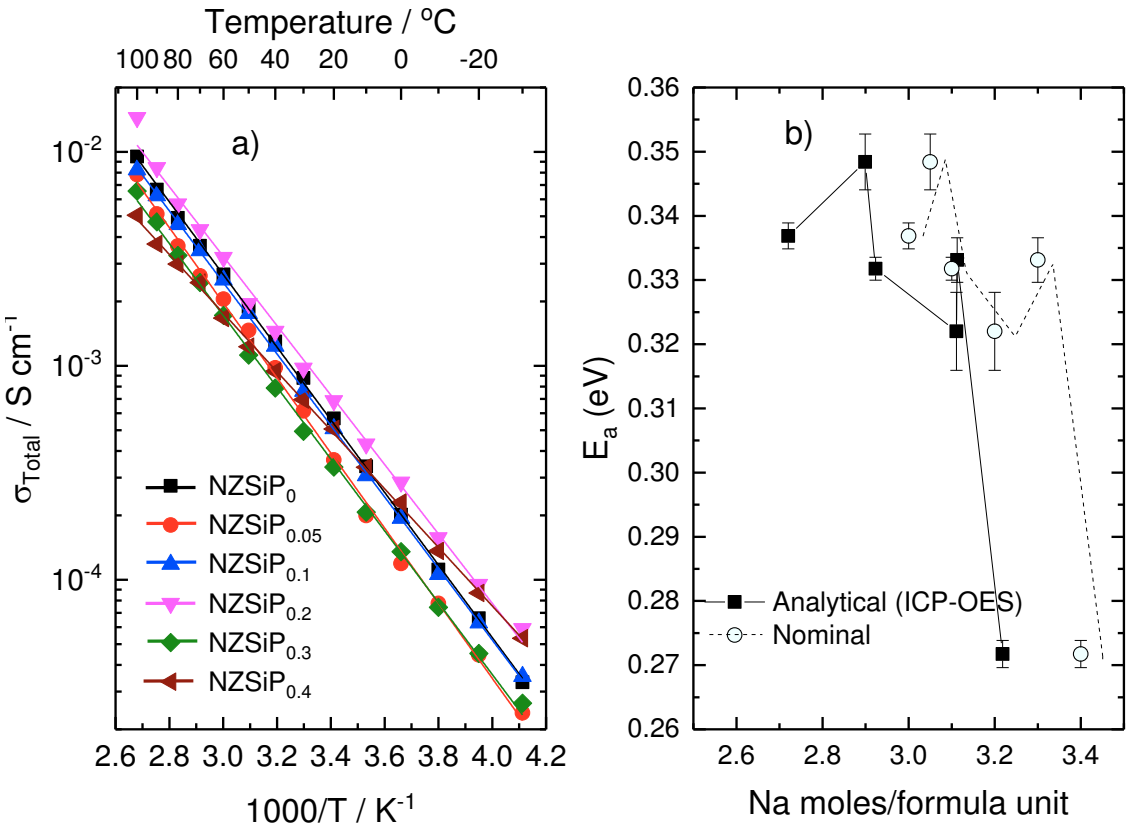

Fig. 7: a) The Arrhenius plot of σ_{total} obtained from impedance spectroscopy in the temperature range -30 – 100 °C and b) the E_a as a function of nominal and analytical composition.

The bulk and grain boundary contribution in σ_{total} was separated using an equivalent circuit. The resulting conductivity data are shown in Fig. 8. Also in the case of σ_{bulk}, the highest conductivity was observed for $Na_{3.2}Zr_2Si_2PO_{12.1}$ with an analytical composition of $Na_{3.11}Zr_{2.01}Si_{1.84}PO_{12}$. On the one hand, the slopes of σ_{bulk} are varying, on the other hand, the slopes of σ_{gb} have similar slopes and they follow an irregular trend.

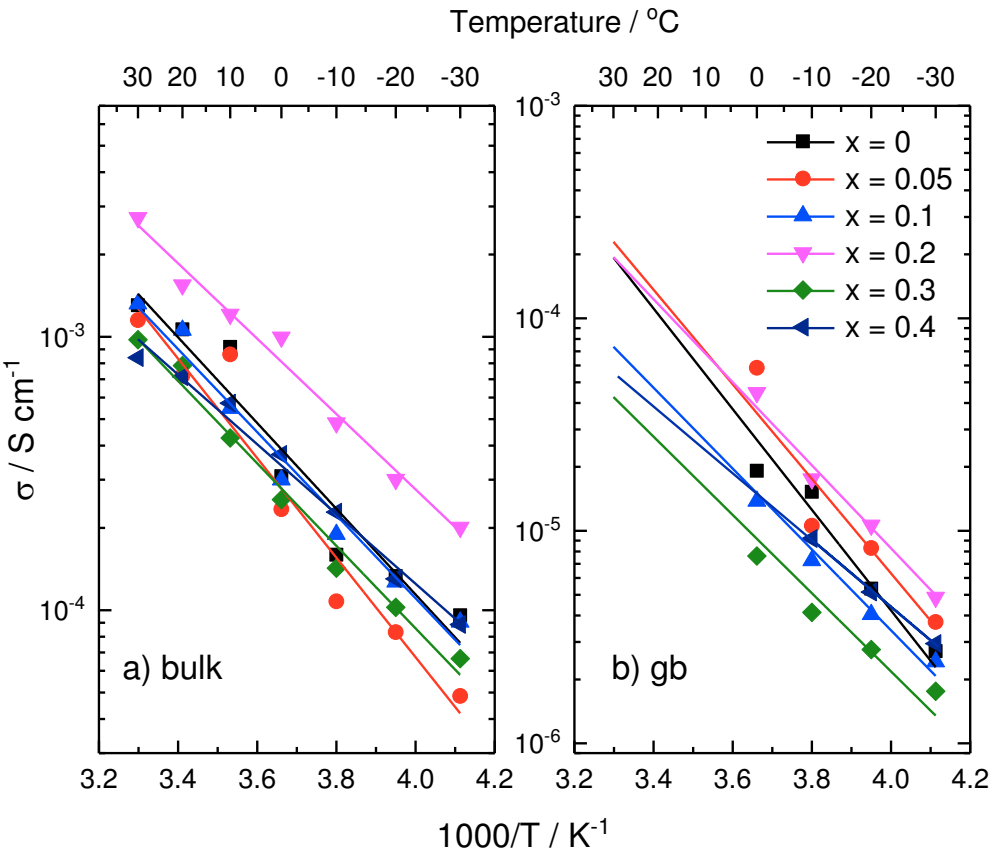

Fig. 8: The Arrhenius plot of σ_{bulk} and σ_{gb} after fitting the equivalent circuit to the impedance data in the range of 30 to -30 °C (extrapolated for σ_{gb} from 0 °C - 30 °C). The lines are linear fits of the data.

The σ_{bulk} and σ_{gb} at 25 °C obtained from Fig. 8 are plotted as a function of *x* in Fig. 9. The figure shows that the maximum σ_{bulk} was observed when the Na excess in the formula unit was 0.2 moles, i.e. $Na_{3.2}Zr_2Si_2PO_{12.1}$. This is the composition where the sodium loss after sintering was very low. Furthermore, when plotted against the analytical stoichiometry, a similar trend is observed. The σ_{gb} was obtained from the ratio of the capacitances of bulk and grain boundaries, as reported earlier [22] and it shows an irregular trend by changing *x* in the series.

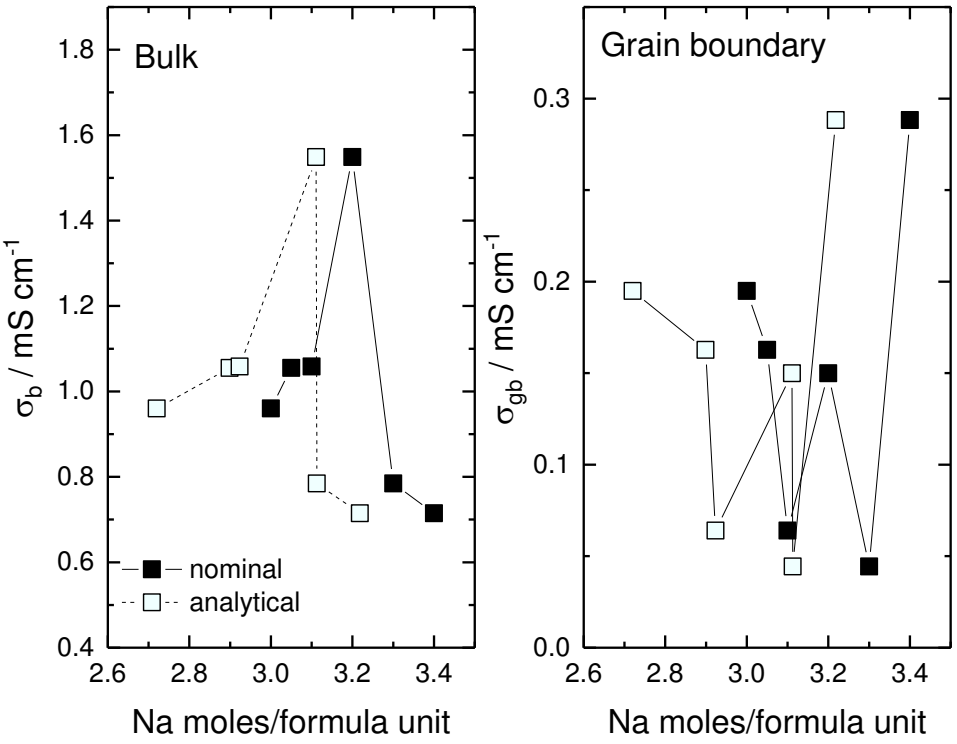

Fig. 9: The bulk and grain boundary conductivity at 25 °C as a function of nominal and analytical Na content per formula unit in $Na_{3+x}Zr_2Si_2PO_{12+x/2}$. The lines are drawn as a guide to the eye.

The E_a of σ_{gb} and σ_{bulk} are plotted against the nominal and analytical stoichiometry in Fig. 10. In case of nominal composition, the nominal Na content per formula unit is not an adequate representation however, if $E_{a,bulk}$ is plotted against the analytical Na content per formula unit, a clear negative slope is observed. Also $E_{a,gb}$ (Fig. 10b) indicates an overall decreasing trend with increase in Na content. The reason for a decreasing trend observed $E_{a,gb}$ requires a detail investigation of the grain boundary chemistry. The formation of glassy phase in all the compositions (see Fig. 5) is in agreement with the phase relations of NaSICON [30]. The tendency of Si or P rich glass phase formation seems to be more pronounced for NaSICON compositions with sodium deficiency. Here the Na content per formula unit varied between 2.72 and 3.22 mole for $x = 0$ and $x = 0.4$, respectively, which means that the tendency of glass phase formation decreases with increasing x in $Na_{3+x}Zr_2Si_2PO_{12+x/2}$. It is already reported that these glassy phases act as barrier towards Na^+ conduction and therefore have high activation energies

[26, 27]. In our case, it is confirmed by a decreasing overall trend of $E_{a,gb}$ with increasing sodium content.

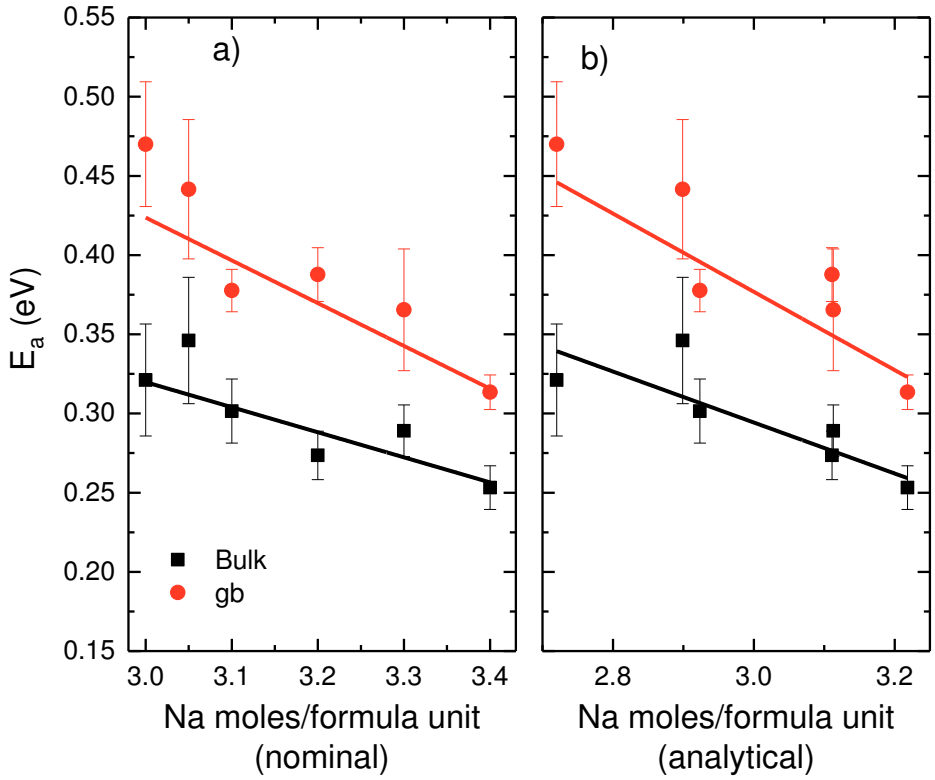

Fig. 10: The E_a of σ_{gb} and σ_{bulk} as a function of a) nominal and b) analytical Na moles per formula unit of $Na_{3+x}Zr_2Si_2PO_{12+x/2}$. The shaded regions are a depiction of the error range.

The reason for a decreasing $E_{a,bulk}$ as a function of Na content per formula unit is explained based on the ratio of Na^+ vacancies/charge carriers in the crystal lattice. It has also been reported earlier that the activation energy of bulk conductivity decreases with an increasing Na content in the NaSICON from 3.0 – 3.4 moles per formula units [6, 8, 11].

In a typical NaSICON-type material like $Na_3Zr_2Si_2PO_{12}$ the site occupancy of Na is 75 % and there are three Na sites in the formula units. These sites are Na(1), sixfold coordinated to oxygen ions of three $(Si,P)O_4$ tetrahedra with coordinate (0,0,0), Na(2) which is also sixfold coordinated to oxygen ions of three coplanar $(Si,P)O_4$ tetrahedra with coordinate (x,y,0.25) and Na(3) with threefold coordination to the oxygen ions of three ZrO_6 octahedra [31]. To achieve high ionic

conductivity, the ratio of charge carriers occupying the Na sites and the Na vacancies has to be optimum. Too high site occupancy would leave no available vacancies for ion hopping and would result in increasing resistance and E_a of ion transport. On the contrary, low site occupancy also leads to high resistance due to less number of charge carriers for ion transport. The Na(1) sites are thermodynamically more stable than the other two. Therefore it is likely that these sites will be preferably filled with the Na^+ ions. Once Na(1) sites are filled, the remaining Na^+ ions are then randomly distributed over the available Na(2) and Na(3) sites [1]. The sodium conduction occurs along two pathways, i.e. Na(1) – Na(2) – Na(1) and Na(1) – Na(3) – Na(1). Based on DFT computations [17], the authors came to the conclusion that Na excess in a monoclinic NaSICON structure increases the bottleneck area between the sites Na(1) and Na(2), which as a consequence results in expedited transport of Na^+ ions in the structure. However, they only studied Na excess with stoichiometries $Na_{3.3}Zr_2Si_2PO_{12.15}$ and $Na_{3.6}Zr_2Si_2PO_{12.3}$, and found out that conductivity is maximum at 3.3 moles of Na per formula unit and lower at 3.6 moles of Na per formula unit.

Guin et al. performed a detailed study of $Na_{3+x}Sc_2Si_xP_{3-x}O_{12}$ and reported that the E_a vs. Na content has a v-shaped curve. The E_a first decreases until the Na content is increased from 3.0 to 3.4 moles per formula unit. For Na contents more than 3.4 moles per formula unit, the E_a began to increase [11]. A similar trend is reported for other solid solutions ($Na_{3+x}Sc_xZr_{2-x}Si_2PO_{12}$ [6] and $Na_{1+x}Zr_2Si_xP_{3-x}O_{12}$ [8]). Likewise, our results are also showing a similar trend assuming the sodium content in the glass phase is negligible and hence, the addition of sodium oxide to $Na_3Zr_2Si_2PO_{12}$ leads to the increase in conductivity and decrease of $E_{a,bulk}$ as long as these materials have a sodium content less than 3.4 moles per formula unit.

Above is true only if we assume that Na excess is occupying only the sodium positions in the NaSICON crystal lattice. Contrary would mean that $Na_{3+x}Zr_2Si_2PO_{12+x/2}$ is not valid or only to a certain limit, and if Na occupies Zr sites the equation becomes $Na_{3+x}Zr_{2-x/4}Si_2PO_{12}$. The Zr substitution would lead to the formation of ZrO_2, which is clearly seen in the microstructure section in Fig. 5. Another form of experimental evidence is difference of white to dark color distribution in the microstructure that is observed in all compositions especially in the grain boundary regions where it becomes darker indicating presence of heavier element in less amount (heaviest element is Zr in $Na_{3+x}Zr_{2-x/4}Si_2PO_{12+x/2}$). This gives more weight to the argument that

any likelihood of Na occupying the Zr sites cannot be ruled out. The only contrary observation to this assumption is in the conductivity measurements by impedance spectroscopy, where a decreasing $E_{a,b}$ is observed with increasing *x* in the series. This would mean that the excess Na is also mobile and it is unlikely that it occupies an immobile Zr site in the lattice.

4. Conclusions

During sintering NaSICON materials undergo significant weight loss due to the evaporation of sodium oxide. Therefore NaSICON materials were prepared with excess of Na with compositions $Na_{3+x}Zr_2Si_2PO_{12+x/2}$ with $0 \leq x \leq 0.4$ and exposed to typical sintering conditions of NaSICON ceramics to study the Na loss. The weight loss is minimized through two-step sintering because the sample is exposed for longer durations are lower temperature (1230 °C). Maximum Na loss observed was 0.4 % for $x = 0.05$ and minimum of 0.07% when $x = 0.2$ for the two-step sintering. Because of low sodium loss, this composition is very close to $Na_3Zr_2Si_2PO_{12}$ and has the highest total and bulk conductivity that reaches 0.9 mS cm^{-1} and 1.6 mS cm^{-1} at 25 °C, respectively. As a general trend the E_a decreases with the increase of Na charge carriers in the investigated range.

5. Acknowledgments

The authors thank Dr. D. Sebold, Dr. Y. J. Sohn, Ms. M.-T. Gerhards and Ms. S. Schwartz-Lückge for SEM investigations, Rietveld refinements, DTA/TG measurements and ultrapycometer investigations, respectively. Financial support from the Ministry of Innovation, Higher Education and Research of North Rhine-Westphalia for the starting funds of the Helmholtz Institute Münster (Az. 433) is gratefully acknowledged.

References

1. Hong, H.Y.P., *Crystal structures and crystal chemistry in the system $Na_{1+x}Zr_2Si_xP_{3-x}O_{12}$.* Materials Research Bulletin, 1976. **11**(2): p. 173-182.
2. Goodenough, J.B., H.Y.P. Hong, and J.A. Kafalas, *Fast Na^+-ion transport in skeleton structures.* Materials Research Bulletin, 1976. **11**(2): p. 203-220.
3. Anantharamulu, N., et al., *A wide-ranging review on NASICON type materials.* Journal of Materials Science, 2011. **46**(9): p. 2821-2837.
4. Catti, M., S. Stramare, and R. Ibberson, *Lithium location in NASICON-type Li conductors by neutron diffraction. I. a' Triclinic -$LiZr_2(PO_4)_3$.* Solid State Ionics, 1999. **123**: p. 173-180.
5. Iglesias, J.E., et al., *Low temperature triclinic distortion in NASICON-type $LiSn_2(PO_4)_3$.* Journal of Solid State Chemistry, 1997. **120**: p. 322-326.
6. Ma, Q., et al., *Scandium-Substituted $Na_3Zr_2(SiO_4)_2(PO_4)$ Prepared by a Solution Assisted Solid-State Reaction Method as Sodium-Ion Conductors.* Chemistry of Materials, 2016. **28**(13): p. 4821-4828.
7. Guin, M., F. Tietz, and O. Guillon, *New promising NASICON material as solid electrolyte for sodium-ion batteries: Correlation between composition, crystal structure and ionic conductivity of $Na_{3+x}Sc_2Si_xP_{3-x}O_{12}$.* Solid State Ionics, 2016. **293**: p. 18-26.
8. Kafalas, J.A. and R.J. Cava, *Effect of pressure and composition on fast Na^+ transport in the sytem $Na_{1+x}Zr_2Si_xP_{3-x}O_{12}$.* Proceedings of Fast Ion Transport in Solids, ed. P. Vashishta, J.N. Mundy, and G.K. Shenoy. 1979: Elsevier North Holland.
9. Kousuke, N., et al., *Liquid-phase sintering of highly Na^+ ion conducting $Na_3Zr_2Si_2PO_{12}$ ceramics using Na_3BO_3 additive.* Journal of the American Ceramic Society, 2018. **101**(3): p. 1255-1265.
10. Krok, F., *Influence of sintering conditions on chemical composition of NASICON.* Solid State Ionics, 1987. **24**(1): p. 21-28.
11. Guin, M., PhD. thesis: *Chemical and physical properties of sodium ionic conductors for solid-state batteries*. 2016, Rheinisch -Westfälischen Technischen Hochschule (RWTH) Aachen.
12. Naqash, S., et al., *$Na_3Zr_2(SiO_4)_2(PO_4)$ prepared by a solution-assisted solid state reaction.* Solid State Ionics, 2017. **302**: p. 83-91.
13. Bale, C.W., et al., *FactSage thermochemical software and databases, 2010–2016.* Calphad, 2016. **54**: p. 35-53.
14. K. Hack, T.J., M. Müller, E. Yazhenskikh, G. Wu. *A novel thermodynamic database for slag systems and refractory materials*. in *5th International Congress on the Science and Technology of Steelmaking, ICS*. 2012. Dresden, Germany, Article no. 13.
15. Maier, J., U. Warhus, and E. Gmelin, *Thermodynamic and electrochemical investigations of the Nasicon solid solution system.* Solid State Ionics, 1986. **18-19**: p. 969-973.
16. Wang, D., et al., *Crystal structure of zirconia by Rietveld refinement.* Science in China Series A: Mathematics, 1999. **42**(1): p. 80-86.
17. Park, H., et al., *Sodium Ion Diffusion in Nasicon ($Na_3Zr_2Si_2PO_{12}$) Solid Electrolytes: Effects of Excess Sodium.* ACS Applied Materials & Interfaces, 2016. **8**(41): p. 27814-27824.
18. Lee, M.J., et al., *Hygroscopic behavior of individual $NaNO_3$ particles.* Atmos. Chem. Phys. Discuss., 2011. **2011**: p. 23203-23229.
19. Mazaheri, M., A. Simchi, and F. Golestani-Fard, *Densification and grain growth of nanocrystalline 3Y-TZP during two-step sintering.* Journal of the European Ceramic Society, 2008. **28**(15): p. 2933-2939.
20. Chen, I.W. and X.H. Wang, *Sintering dense nanocrystalline ceramics without final-stage grain growth.* Nature, 2000. **404**(6774): p. 168-171.
21. Feng, P., et al., *A novel two-step sintering for nano-hydroxyapatite scaffolds for bone tissue engineering.* 2014. **4**: Article no. 5599.
22. Naqash, S., et al., *Microstructure–conductivity relationship of $Na_3Zr_2(SiO_4)_2(PO_4)$ ceramics.* Journal of the American Ceramic Society. **https://doi.org/10.1111/jace.15988**.

23. Lee, S.M., et al., *Effect of particle size on the density and ionic conductivity of $Na_3Zr_2Si_2PO_{12}$ NASICON.* Journal of Ceramic Processing Research, 2015. **16**(1): p. 49-53.
24. Kuriakose, A.K., et al., *Synthesis, Sintering, and Microstructure of Nasicons.* Journal of the American Ceramic Society, 1984. **67**(3): p. 179-183.
25. Fuentes, R.O., F.M.B. Marques, and J.I. Franco, *Synthesis and properties of nasicon prepared from different zirconia-based precursors.* Boletín de la Sociedad Española de Cerámica y Vidrio 1999. **38**(6): p. 631-634.
26. Kang, H.-B. and N.-H. Cho, *Phase formation, sintering behavior, and electrical characteristics of NASICON compounds.* Journal of Materials Science, 1999. **34**(20): p. 5005-5013.
27. Boilot, J.P., P. Colomban, and G. Collin, *Nasicon : Amorphous to crystalline compounds.* Solid State Ionics, 1986. **18-19**(PART 2): p. 974-980.
28. Khireddine, H., et al., *Optimization of NASICON composition for Na^+ recognition.* Sensors and Actuators B-Chemical, 1997. **40**(2-3): p. 223-230.
29. Ahmad, A., et al., *Dependence of the properties of Nasicons on their composition and processing.* Solid State Ionics, 1987. **24**(1): p. 89-97.
30. Tietz, F., *Phase relations of NASICON materials in the quaternary phase diagram.* AIMS Material Science, 2017. **4**(6): p. 1305-1318.
31. Vogel, E.M., R.J. Cava, and E. Rietman, *Na^+ ion conductivity and crystallographic cell characterization in the Hf-nasicon system $Na_{1+x}Hf_2Si_xP_{3-x}O_{12}$.* Solid State Ionics, 1984. **14**(1): p. 1-6.